Development of a laser for chirp cooling of positronium to near the recoil limit using a chirped pulse-train generator

Kenji Shu [ORCID],[1,2,3] Naoki Miyamoto,[2] Yuto Motohashi [ORCID],[3] Ryosuke Uozumi [ORCID],[2] Yohei Tajima,[2] and Kosuke Yoshioka [ORCID][1,2,3,*]

[1]*Photon Science Center, School of Engineering, The University of Tokyo, 2-11-16 Yayoi, Bunkyo-ku, Tokyo 113-0032, Japan*
[2]*Department of Applied Physics, School of Engineering, The University of Tokyo, 7-3-1 Hongo, Bunkyo-ku, Tokyo 113-8656, Japan*
[3]*Department of Applied Physics, Faculty of Engineering, The University of Tokyo, 7-3-1 Hongo, Bunkyo-ku, Tokyo 113-8656, Japan*

We present the development and characterization of a pulsed 243-nm laser designed for cooling positronium (Ps) to near the recoil limit. The laser, based on the recent chirped pulse-train generator (CPTG) demonstrated by Yamada *et al.* [K. Yamada *et al.*, Phys. Rev. Appl. **16**, 014009 (2021)], outputs a train of pulses with spectral widths of 10 GHz. The center frequency of each pulse is shifted upward (up-chirped) in time by 4.9×10^2 GHz μs^{-1}. These parameters are determined by the mechanism of chirp cooling, a suitable scheme for cooling numerous Ps atoms to the recoil temperature of laser cooling. To achieve the desired performance, we drove an optical phase modulator in the CPTG with a high modulation depth based on the operating principle of the cooling laser. Time-resolved spectroscopic measurements confirmed that the developed laser satisfies the chirp rate and instantaneous spectral width requirements for efficient chirp cooling. We believe that the experimental demonstration of Ps laser cooling with a pulse energy of hundreds of microjoules has become possible using realistic methods for the generation and velocity measurement of Ps.

I. INTRODUCTION

Positronium (Ps), which is the bound state of an electron and a positron, is a unique system for precise investigation of fundamental physics [1,2]. Its purely leptonic composition allows precise calculations of eigenenergies and lifetimes. Comparisons between the calculated energy intervals and their precise measurements can be stringent tests of quantum electrodynamics and probes for new physics, such as the asymmetry between matter and antimatter. For most intervals between the energy levels of Ps, the measurement precision is currently inferior to that of calculations [2–6]. One difficulty in these spectroscopic measurements arises from the light mass of Ps. As Ps is the lightest atom, its velocity distribution is very broad at typical temperatures, which dominantly contributes to measurement errors in both the optical and microwave regions [4,6]. Consequently, the cooling of Ps will be a breakthrough achievement in increasing the measurement precision and even in achieving Bose-Einstein condensation (BEC) combined with a dense cloud of Ps [7–9]. The conventional cooling technique uses thermalization processes between energetic Ps atoms and cryogenic materials [10,11]. The lowest temperature of the Ps atom clouds emitted into vacuum is currently limited to approximately 100 K [10,12,13].

Laser cooling is a promising technique for cooling Ps to temperatures significantly lower than the current limit [14–16]. One advantage is the large recoil velocity achieved by absorbing the momentum of a photon because of its light

mass. This is particularly important for Ps, which is an unstable atom with a decay lifetime of 142 ns in the long-lived $1\,^3S_1$ state [17,18]. Rapid cooling of initially hot Ps is considered possible using the $1S$-$2P$ transition in a time duration comparable to its lifetime. However, the light mass makes it difficult to prepare an appropriate laser. A laser at a wavelength of 243 nm with both a broadband spectrum and long duration is required. Recently, some of the authors of this paper proposed an operating principle for a laser that can potentially enable chirp cooling of Ps [9,19]. Although our experiment demonstrated the validity of the proposed principle [19], the developed laser system requires significant advancements to achieve efficient cooling, based on the principle of chirp cooling. As we show in this paper, the chirp rate and instantaneous spectral width of the laser are crucial for cooling the majority of a thermal Ps atom gas to the fundamental limit of laser cooling. Those parameters of the proof-of-principle system should be enhanced by an order of magnitude.

In this paper, we demonstrate significant enhancements of the chirp rate and instantaneous spectral width of the chirped pulse-train generator (CPTG) for laser cooling of Ps to near the recoil limit. We show that, based on the working principle of the CPTG, the desired enhancements can be achieved if the driving power of the optical phase modulator utilized in the CPTG can be increased by an order of magnitude. The pulsed driving of the modulator represents a breakthrough to achieve the required driving power without damaging any components in the modulator. The improved phase modulation technique supports the possibility of optimizing the CPTG for Ps laser cooling. We also qualitatively discuss the specifications required for a laser to perform efficient chirp cooling of Ps; moreover, we developed such a laser based

*yoshioka@fs.t.u-tokyo.ac.jp

on the significantly enhanced CPTG with those specifications. The developed laser was directly characterized in the time and spectral domains via methods superior to those employed in the previous work, and it was confirmed that the laser met the requirements for cooling Ps to the limit posed by recoil from emitted photons during the process of laser cooling. The cooling method utilizing the developed laser provides an approach to realize Ps atom gas cooling to sub-Kelvin temperatures.

II. CONCEPT OF THE DESIGN

A. Proposal of Ps chirp cooling

We first review how laser cooling of Ps works within a duration comparable to the lifetime of Ps, according to previous studies [9,14–16]. Those studies stated that a cooling laser with a broadband spectrum could be useful for cooling many Ps atoms, but we note that this configuration with a laser intensity comparable to the saturation intensity of the transition limits the reachable temperature of laser-cooled atoms to several degrees Kelvin. In this paper, we propose an efficient chirp cooling method for Ps to achieve a velocity distribution as narrow as practically limited by the recoil effect. Previous studies considered laser cooling using a pulsed laser with a wavelength of 243 nm, which has a long time duration on the order of 100 ns, and a broadband spectrum on the order of 10 or 100 GHz. The wavelength is resonant with the transition between the $1S$ and $2P$ states. The $1S - 2P$ transition is the most suitable for laser cooling because of its short spontaneous emission lifetime of approximately 3.2 ns and its long lifetime for decay to gamma rays [20]. The required time duration can be estimated from the typical initial velocity of Ps, the effective rate at which spontaneous emission occurs, and the recoil velocity. For example, the most probable velocity of the cloud of Ps in the Maxwell-Boltzmann distribution at the temperature T in degrees Kelvin is $3.8 \times 10^3 \sqrt{T}$ m/s. When the transition is strongly induced to saturation, the effective rate of the cooling cycle is $\frac{1}{2} \times \frac{1}{3.2 \, \text{ns}}$. The recoil velocity for the 243-nm photon is 1.5×10^3 m/s. Therefore, the duration required to cool Ps to the cooling limit was calculated to be $16\sqrt{T}$ ns. Cooling of Ps from several hundred degrees Kelvin can be accomplished in a time duration on the order of 100 ns, which is comparable to the lifetime of spin-triplet Ps. This rapid cooling is possible because of the high recoil velocity, which originates from the light mass of Ps. A pulsed laser with this long duration, rather than a continuous-wave oscillation, is preferable to achieve sufficient intensity at the UV wavelength of 243 nm to maximize the effective rate of spontaneous emissions with a typical laser beam size to cover the size of a gaseous cloud of Ps. The broadband spectrum is required to cool numerous Ps atoms. The Doppler width at the thermal equilibrium is $27\sqrt{T}$ GHz at the full width at half maximum (FWHM) at T K. Therefore, a spectral width on the order of 10 or 100 GHz is necessary for cooling Ps gas at an initial temperature of hundreds of degrees Kelvin.

The broadband spectrum of the cooling laser is useful for cooling many Ps atoms, but assuming a typical smooth spectrum shape, it also limits the narrowness of the resulting cooled Ps velocity distribution. In previous studies discussing the laser cooling process of Ps with the best realistically

obtainable lasers at that time [15,16], the spectra of lasers were assumed to be broadband, smooth, and fixed. Figure 1(a) illustrates a simulated Doppler profile after cooling with such a laser spectrum from an initial temperature of 300 K. The laser was assumed to have linear polarization and be irradiated by the counterpropagating configuration for 200 ns. The simulation was done using the code that we developed for chirp cooling simulation, which was based on the Bloch equation formalism and will be explained in detail later. In this case, the frequency detuning should be as large as the broad spectral width of the laser to suppress the photon absorption process, which leads to the acceleration of Ps. This hinders achieving a narrow velocity distribution of laser-cooled Ps. The width of the resulting Doppler profile is approximately 50 GHz or 4 K in temperature, which is comparable to the laser spectral width of 75 GHz in the simulation. Given that twice the Doppler shift with the recoil velocity is around 12 GHz, as demonstrated in the following paragraphs, the simulated Doppler profile is approximately four times wider than the recoil limit. Reducing the spectral width would help to reach the recoil limit, but it would also reduce the number of Ps atoms that can be cooled. The simulation assumed a detuning of 75 GHz, consistent with [16], along with the spectral width. The averaged intensity during cooling was $0.45 \, \text{kW cm}^{-2}$, saturating the transition. The frequency mode interval was set to 40 MHz, ensuring an effectively continuous laser spectrum considering the natural linewidth of the employed transition.

Here, we propose a chirp cooling scheme, in which the frequency of the laser shifts in time (chirps), that would both cool many Ps atoms and achieve the minimum reachable temperature. Chirp cooling is a powerful technique capable of cooling a broad range of initial velocities of prepared atoms by adjusting the laser frequency to resonate with the atoms being decelerated. This technique has found different applications, such as stopping hot or fast atomic beams [21,22]. The first theoretical work on laser cooling of Ps [14] suggested that chirp cooling could be valuable for this purpose. However, it posited that achieving the necessary chirp rate for cooling Ps was challenging at that time, providing no detailed discussions on chirp cooling. Instead, it estimated that using a broadband laser with a steep cutoff at the blue side could cool Ps to around or below the recoil limit temperature. Yet, no reports have been made thus far on developing such a laser or conducting a cooling experiment. In the following sections, we elucidate how efficient Ps chirp cooling operates as an alternative method to approach the recoil limit. The physics for determining the appropriate chirp rate and instantaneous spectral width is also presented. The appropriate instantaneous spectral width is required to balance the amount and temperature of cooled Ps. The importance of this parameter has not been discussed in previous literature [14].

The chirp cooling method proves advantageous in achieving a narrow instantaneous spectral width for the laser. The spectrum of such a laser and a simulated Doppler profile post-cooling are illustrated in Fig. 1(b). In contrast to the previously discussed scenario, the laser detuning at the conclusion of the cooling process can be minimized. With the confirmed parameters of the laser in both time and frequency domains, reported in this paper, the simulation anticipates that the width of the
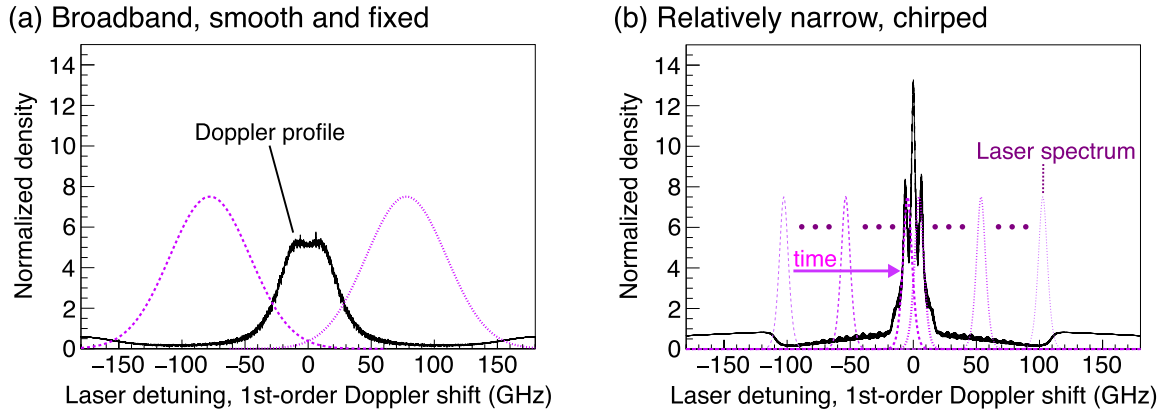
FIG. 1. Comparison of laser cooling schemes using a laser with a smooth and fixed spectrum and a chirped laser, showing the laser spectra (dashed and dotted curves) and simulated Doppler profile (solid curves) after cooling. For the laser spectra, the horizontal axis shows the laser detuning from $f_R = 1\,233\,596$ GHz, which corresponds to the average of energy differences between $1\,^3S_1$ and $2\,^3P_J$ states weighted by each multiplicity of the excited state. The Doppler shift Δf_D shown in the horizontal axis was related with Ps velocity v_{Ps} by $\Delta f_D = f_R v_{Ps}/c$. (a) Case in which the laser spectrum is smooth and fixed. The broadband spectrum is required to be resonant for Ps atoms with a wide range of velocity. The detuning should be as large as its broad spectral width to avoid laser heating. (b) Case in which a chirped pulse train is used. The narrow instantaneous spectral width in chirp cooling allows smaller detuning at the end of the cooling.

resulting Doppler profile would be approximately 10 GHz, nearing the recoil limit. The average intensity during the cooling period was set to 1 kW cm^{-2} to saturate the transition.

A narrow laser spectrum with frequency chirp can be useful for Ps chirp cooling as the frequency detuning at the end of the cooling process can be small, but if it is excessively narrow, the cooling efficiency will degrade. One cause for this is that the recoil in random directions caused by photons from spontaneous emissions broadens the velocity distribution of laser-cooled Ps. This occurs even after a single cycle of the cooling process, as the laser cooling schemes of Ps proposed so far require spontaneous emissions. The random Doppler shifts resulting from a single cooling cycle spread uniformly over $2\Delta_r = 2\frac{\hbar k_p^2}{2\pi m_{Ps}}$; k_p is the wave number of an emitted photon, m_{Ps} is the mass of Ps, and $\hbar$ is the reduced Planck constant. Preferably, the laser spectrum should be comparably broad relative to $2\Delta_r$ to achieve resonance with most Ps atoms under cooling. The other reason causing poor cooling efficiency in the case of an excessively narrow spectrum is the energy splitting of the $2\,^3P_J$ ($J = 0, 1, 2$) states of Ps, as depicted in Fig. 2, which also shows the Doppler width induced by the recoil. If the laser spectrum also covers this splitting, it can excite all possible transitions for laser cooling. One benefit of this approach is that the transition strength can be increased for efficient laser cooling, and another is that we can avoid Ps atoms becoming polarized by an optical pumping process. An optimal value exists for the instantaneous spectral width to balance the quantity and temperature of cooled Ps atoms.

From this qualitative consideration of the Ps cooling scheme using the chirped pulse train, an appropriate chirp rate and instantaneous spectral width exist. In this paper, we semiquantitatively determine these values using fundamental parameters. The appropriate chirp rate can be determined from the shift of the resonance frequency Δ_r caused by the absorption of a single laser photon and the effective duration required (6.4 ns) to complete a single cooling cycle. With $k_p = 2\pi/243$ nm, Δ_r is approximately 6.2 GHz.

If the laser chirps 6.2 GHz every 6.4 ns, the chirp rate will be approximately 1×10^3 GHz μs^{-1}. We assume the appropriate chirp rate is less than this value and on the order of 100 GHz μs^{-1}, as not all Ps atoms can be decelerated in a single cooling cycle due to the randomly distributed Doppler shifts resulting from spontaneous emissions. A spectral range swept by this order of chirp rate during the lifetime of spin-triplet Ps can be up to 100 GHz, which is comparable to the initial Doppler width of typical Ps atom gas. With respect to the instantaneous spectral width, the appropriate value is assumed to be approximately 10 GHz, considering both the randomly distributed Doppler shifts $2\Delta_r \simeq 12.4$ GHz in cooling cycles and the splitting of the $2P$ states, which is 9.9 GHz at maximum. The ideal width should be determined such that it provides a balance between the cooled fraction and final temperature of cooled Ps, as discussed above. In the time domain, a pulse width close to the Fourier-transform limit is anticipated from the principle of operation of this laser. An instantaneous spectral width of 10 GHz in the frequency spectrum suggests a short pulse lasting between 10 and 100 ps depending on the actual spectral shape. Because the chirp
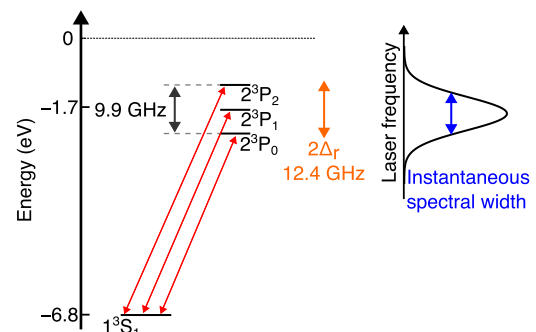

FIG. 2. Level diagram including the $1\,^3S_1$ and $2\,^3P_J$ states of Ps, the Doppler width resulted by the recoil, and a laser spectrum for inducing all transitions between $1\,^3S_1$ and all sublevels in the excited states.

cooling continues for hundreds of nanoseconds, our cooling scheme can be realized with a train of such short pulses with their central frequencies shifting sequentially. The CPTG can potentially emit this chirped pulse train [19]. We designed a significant enhancement of the previously developed CPTG for achieving the assumed appropriate chirp rate and spectral width of a single pulse according to the working principle reported in [19]. The realization of deep frequency modulation with a time-dependent depth is a key technological advancement. In the next subsection, we discuss how this became possible, including a brief review of the CPTG.

Further accurate determination of optimized laser parameters could be achieved through numerical simulations, as conducted in [16]. However, the chirp cooling scheme we propose using the train of pulses precludes the adoption of existing formalisms based on rate equations. For the sake of rapid cooling of Ps, the intensity of each pulse from the CPTG has to be appropriately high to enhance the excitation probability, and the pulse interval should be comparable to the 3.2-ns spontaneous emission lifetime. In this case, mutual coherence between pulses and its effect on cooling dynamics cannot be neglected. As also previously discussed [16], interactions between Ps and photons in such a laser necessitate the incorporation of the coherence term in Bloch equation formalism. The applicability of the rate equation formalism is established in simulations of cooling under the irradiation of incoherent and broadband lasers [16], which is not the case for the CPTG. Irradiation with multiple high-intensity short pulses at intervals shorter than the decoherence time can induce coherence-related phenomena beyond the predictions of rate equation formalism, such as Ramsey interference. Depending on the parameter setting of our cooling laser, the influence of such coherence on cooling cannot be neglected, and the effect is difficult to predict intuitively. Therefore, we developed a simulation code based on Bloch equation formalism for the accurate modeling of the Ps-photon interaction. The time evolution of the density matrix was traced according to the Lindblad master equation [23]. The considered quantum state space had basis states that were labeled by the internal state of Ps including the spin-triplet $1S$ and $2P$ states and the translational momentum. The Ps-photon interaction was considered up to the electric dipole interaction. The laser field was described as a coherent state with a very large average photon number, and changes in the photon number due to Ps-photon interactions were neglected. The spontaneous emission and decay by self-annihilation were included in the dissipative part of the Lindbladian. To address the extensive momentum state space required for simulating laser cooling of a typical Ps atom cloud, whose initial Doppler profile is orders of magnitude wider than the natural linewidth of the employed transition, the simulation was conducted on a supercomputer. Doppler profiles in Fig. 1 were simulated in this manner. A detailed publication outlining the implementation, results, and interpretations of the numerical simulation based on Bloch equation formalism shall be available elsewhere.

B. Design of the laser

A laser with appropriate properties for the chirp cooling of Ps can be achieved by enhancing the spectral features of the

CPTG, the details of which are described in [19]. A schematic of the laser system is shown in Fig. 3. The injection-seeded pulsed laser with an optical phase modulator introduced inside the laser cavity is called the chirped pulse-train generator because it emits a train of optical pulses with a short duration, whose carrier frequencies are shifted by each pulse. According to the modeled dynamics of the laser oscillation [19], the spectral width of each pulse is $\beta \Omega_{\mathrm{m}} F \ln 2/(2\pi)$ at FWHM, and its center angular frequency shifts over time at a rate of $\Omega_{\mathrm{m}} \beta / T_{\mathrm{trip}}$. Here, β is the modulation depth, Ω_{m} is the modulation angular frequency of an electro-optic modulator (EOM) inside the laser cavity, F denotes the laser cavity finesse, and T_{trip} is the round-trip time of the laser cavity. The spectral width after the third harmonic generation (THG) to the desired wavelength of 243 nm experiences broadening, depending on the spectral shape within a single pulse. The chirp rate also triples after the THG. In the time domain, a long cavity length (3.8 m) and a relatively high reflectivity of the output coupler (98%) can be employed to accommodate the long photon lifetime of the optical pulses circulating inside the laser cavity. The duration of the pulse train exceeded 600 ns at FWHM, proving to be sufficiently long for chirp cooling. The modulation angular frequency Ω_{m} and depth β were determined to obtain an optimized spectrum for Ps chirp cooling. Ω_{m} was set as an integer multiple of the longitudinal mode interval of the laser cavity such that the sidebands were also resonant with the cavity modes. The interval was approximately 78.8 MHz for the current laser system. The other parameters related to Ω_{m} include the driving power and frequency of the second EOM, which was placed outside the laser cavity to modulate the output of the CPTG. This EOM was used to make the laser spectrum sufficiently dense for Ps, which has a natural spectral width of approximately $\Gamma_{\mathrm{nat}} = 2\pi \times 50$ MHz in the $1S - 2P$ transition. The CPTG output, whose spectrum is discrete with an interval of $\Omega_{\mathrm{m}}/(2\pi)$, should be deeply phase modulated to fill the interval such that the frequency interval after the second EOM is less than or comparable to $\Gamma_{\mathrm{nat}}/(2\pi)$. A comparison between the natural spectral width and the interval of the discrete spectrum of the laser is presented in Fig. 4. We adopted $\Omega_{\mathrm{m}} = 2\pi \times 236$ MHz $= 2\pi \times 78.8$ MHz $\times 3$ to balance the rapid chirp rate and difficulty of the second modulation. Because a frequency shift occurs for each T_{trip} interval and it exceeds the duration of a cooling cycle when the transition is saturated, the required chirp rate with the current condition is $\Delta_{\mathrm{r}}/T_{\mathrm{trip}} = 0.49$ GHz/ns, which is an order of magnitude higher than that achieved in [19]. The modulation depth corresponding to this chirp rate is $\beta = 8.8$ rad. Using this β value, the spectral width of a single pulse that constitutes the output of the CPTG in the fundamental wave is 22 GHz, which is broader than the target value. Both requirements should be satisfied by dynamically controlling β at a certain low value while operating the EOM before the laser excitation, and at the required level for a rapid chirp thereafter.

III. PULSED DRIVING OF THE EOM FOR ENHANCING THE SPECTRAL BROADENING

We adopted a free-space resonantly enhanced EOM for the modulator inside the laser cavity to achieve the required chirp
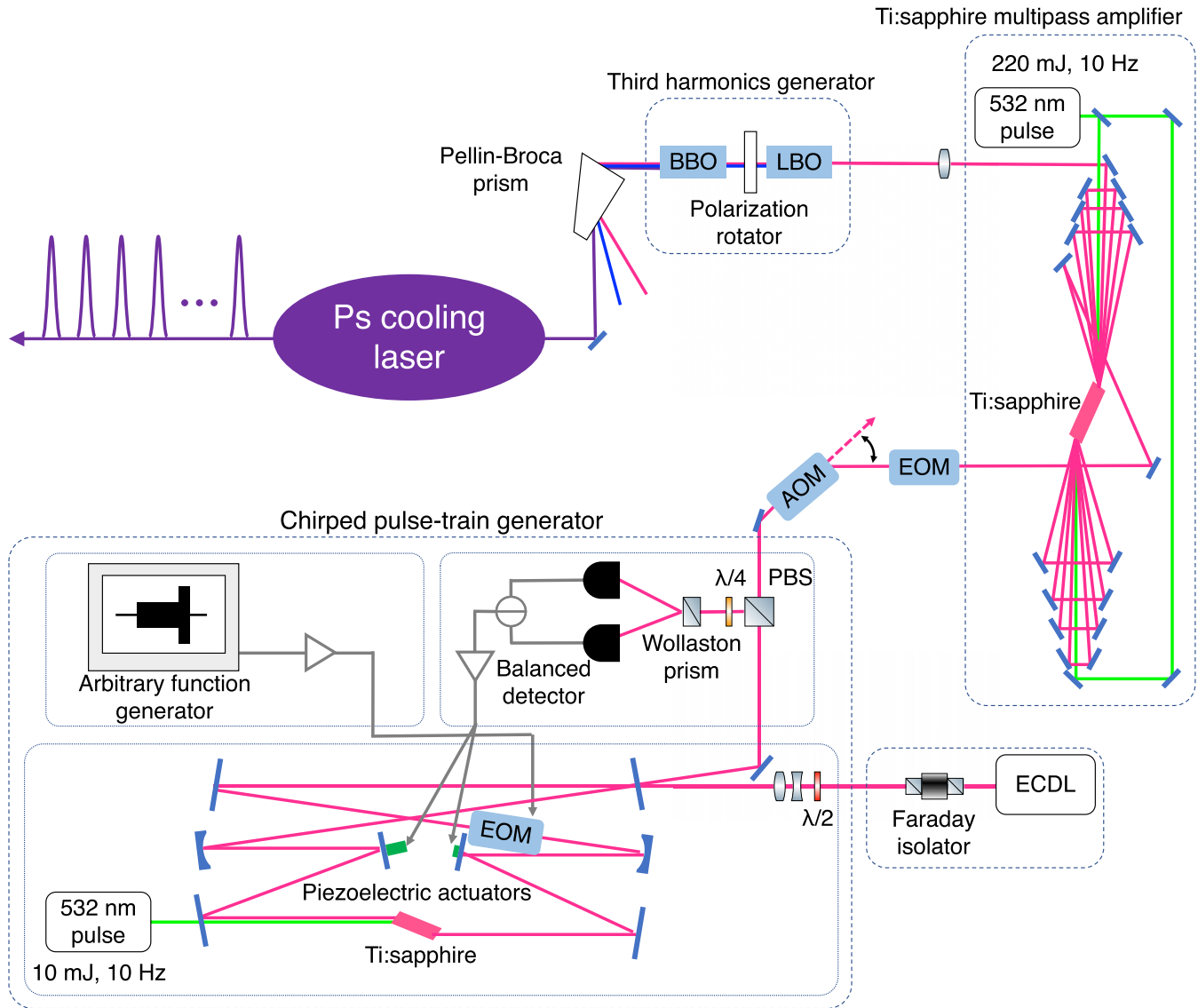
FIG. 3. Schematic of the laser system. The Ti:sapphire pulsed laser is injection seeded by the external cavity diode laser (ECDL), which is a 729-nm continuous-wave (CW) laser, so that the required 243-nm laser can be obtained after the Ti:sapphire multipass amplifier and third harmonic generation (THG) by the lithium triborate (LBO) and beta barium borate (BBO) nonlinear crystals. By driving the electro-optic modulator (EOM) inside the laser cavity, the CPTG outputs a train of pulses. Each pulse has a broad spectral width and carrier-frequency chirp. The output of the CPTG is then diffracted by an acousto-optic modulator (AOM) before being sent to the subsequent stages. The desired part of the CPTG output can be processed by controlling the timing of the pulsed drive of the AOM and the excitation of the multipass amplifier. This pulse chopping can control the duration of the pulse train, which was also used for time-resolved spectroscopy of the laser in this paper. The output is also modulated by the second EOM to make the spectrum dense for the $1S - 2P$ transition of Ps.

rate and single-pulse spectral width. The free-space type was selected because of its low insertion loss, which is necessary for the high finesse of the laser cavity. The EOM used in this paper consists of a KTiOPO$_4$ (KTP) EO crystal with dimensions of $3 \times 3 \times L6$ mm and was manufactured to have a low insertion loss at the working wavelength of 729 nm by using a high-quality crystal and antireflective coating. The finesse of the laser cavity with the EOM was measured as approximately 97. The enhancement in the modulation through resonance can be useful for achieving the required deep modulation because we drive the EOM at a single frequency of 236 MHz. The designed Q factor of the resonant circuit was 98, which indicated that the power of the driving rf signal required to re-

alize $\beta = 8.8$ rad was 25 W. Heat management for this high rf power was unnecessary because we drove the EOM for 16 μs at a repetition rate of 10 Hz, which corresponded to a duty ratio of 1.6×10^{-4}. The modulation bandwidth for the driving rf was 2.4 MHz, which was limited by the Q factor. This bandwidth was wide enough to increase the rf power during the buildup time of the CPTG of several hundred nanoseconds. The modulation depth can then be adjusted to achieve the required chirp rate and spectral width of a single pulse.

We tested whether the required modulation depth, which is too large for free-space EOMs with continuous driving, could be achieved in a pulsed operation. The EOM was driven by a pulsed 236-MHz rf signal, and the modulation
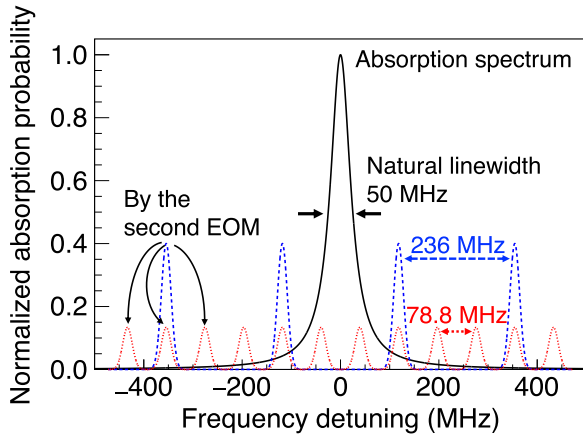
FIG. 4. Comparison between the natural spectral width of the $1S - 2P$ transition of Ps and the interval of the discrete spectrum of the laser. The absorption spectrum of Ps that is broadened by the natural spectral width of approximately 50 MHz is shown as a centered solid curve. Because the developed CPTG has a discrete spectrum with an interval of 236 MHz (dashed curves), there are many Ps atoms whose resonant frequencies are shifted by the Doppler effect and are off-resonant with any spectral component of the laser. Therefore, we generated sidebands with a modulation frequency around the natural spectral width to make the spectrum dense for the transition of Ps. We adopted 78.8 MHz as the modulation frequency for the second EOM, which is one-third of the interval of the unmodulated spectrum. The spectra of the modulated laser are shown by the dotted curves.

depth was measured by analyzing the spectral broadening imposed on the single-longitudinal-mode (SLM) continuous-wave laser. The modulated laser beam was injected into a scanning Fabry-Pérot interferometer (1.5-GHz free spectral range (FSR), >200 finesse), whose cavity length was swept such that its longitudinal modes were swept at a rate of $4 \, \mathrm{MHz \, s^{-1}}$. Because the EOM was driven at a repetition rate of 10 Hz, the optical frequency transmitted through the interferometer was shifted by 0.4 MHz per driving pulse. The transmittance through the interferometer was measured for 40 μs using photodetectors (350-MHz bandwidth), whose outputs were recorded at 1.25 GSa/s with the EOM driven at 10 μs after the beginning of the measurement. The duration of driving the EOM was 20 μs. The optical spectrum was measured by sweeping the interferometer for 1800 s, and the modulation depth was estimated from the distribution of the sideband power. Figure 5 shows the ratio of each sideband power to the incident power on the EOM, as a function of the amplitude of the driving rf signal. We were able to identify up to the ninth-order sideband, and the relationships between the sidebands were consistent with the theoretical model described by the Bessel functions $J_n(\beta)$, where n is the sideband order. In the panel of the kth sideband, the theoretical function is $|J_k(F_{\mathrm{conv}} V_{\mathrm{pp}})|^2$. F_{conv} is the linear conversion factor from the rf amplitude V_{pp} to β, and is the same for all sideband orders. F_{conv} that satisfactorily explains the measured ratios of each sideband power to the incident power was 0.080 rad/V_{pp}. The EOM worked properly up to the maximum driving amplitude, giving $\beta = 9.3 \, \mathrm{rad}$. This is more than the depth required to achieve the optimal chirp rate.

To dynamically control the modulation depth to realize both the optimal spectral width of a single pulse and chirp rate, we adopted an arbitrary function generator (AFG) as the source of the driving rf signal. The AFG outputs a sinusoidal wave at 59 MHz, the amplitude of which is modulated by a square-wave envelope. The amplitude was increased at the timing of the laser excitation of the CPTG. The output frequency was then quadrupled by two serialized doublers, followed by a bandpass filter to allow frequency components around 236 MHz. The 236-MHz pulse was amplified using a low-noise amplifier and a 50-W power amplifier. The typical peak-to-peak amplitudes of the resulting rf signals needed to obtain the required laser spectrum were 30 and 141 V. The latter amplitude was greater than 110 V, which corresponded to $\beta = 8.8 \, \mathrm{rad}$ and provided the required chirp rate. This was due to the slow rise time of the amplitude modulation of approximately 400 ns, which was attributed to the response of the multipliers and filters. With this larger amplitude, we expected that the required β for the chirp rate could be obtained immediately after the buildup of the CPTG.

It is noteworthy that a modulation that is too deep in the buildup period of the CPTG prevents the chirped pulse train from oscillating. This was observed by driving the EOM with a constant amplitude. By increasing β, we observed that pulses oscillated with a larger frequency shift from the seed laser, but in ranges greater than $\beta \simeq 6 \, \mathrm{rad}$ range those pulses became weak and disappeared, and other pulses appeared dominantly at the seed frequency. The frequency shift of the newly appearing pulses increased again when β was further increased. The smaller frequency shift from the seed laser indicates that the newly appearing pulses experienced fewer circulations in the cavity. This can be explained by pulses whose frequency is shifted excessively from that of the seed laser, becoming off-resonant with the cavity. In this case, the newly injected seed laser after the excitation becomes dominant in consuming the gain of the laser medium via the stimulated emissions. The off-resonance of the largely shifted light originates from the unequally spaced longitudinal modes of the laser cavity, which are caused by the dispersive elements. The longitudinal mode interval becomes detuned from the modulation frequency. Sidebands generated in this region cannot interfere constructively with the electric fields that experience different numbers of circulations. The EO crystal dominantly contributes to the dispersion by as much as $1 \times 10^4 \, \mathrm{fs^2}$ in the current setup. This dispersion can limit the spectral width of a single pulse; however, using the theoretical model, the maximum spectral width available by limiting $\beta \simeq 6 \, \mathrm{rad}$ can be estimated as 15 GHz, even in the fundamental wave. This width is broader than 10 GHz, which is the required value for the chirp cooling of Ps. The described off-resonance problem can be neglected if a significant increase in β occurs after excitation of the CPTG. The power of a sufficiently built-up pulse train in the laser cavity can be very high when compared with that of the seed laser injected after the excitation. Therefore, the gain of the laser medium is consumed by the original pulse train. This holds true for our laser system, where we apply the amplitude modulated rf pulse. Thus, the maximum depth of modulation can be applied to achieve the required chirp rate.
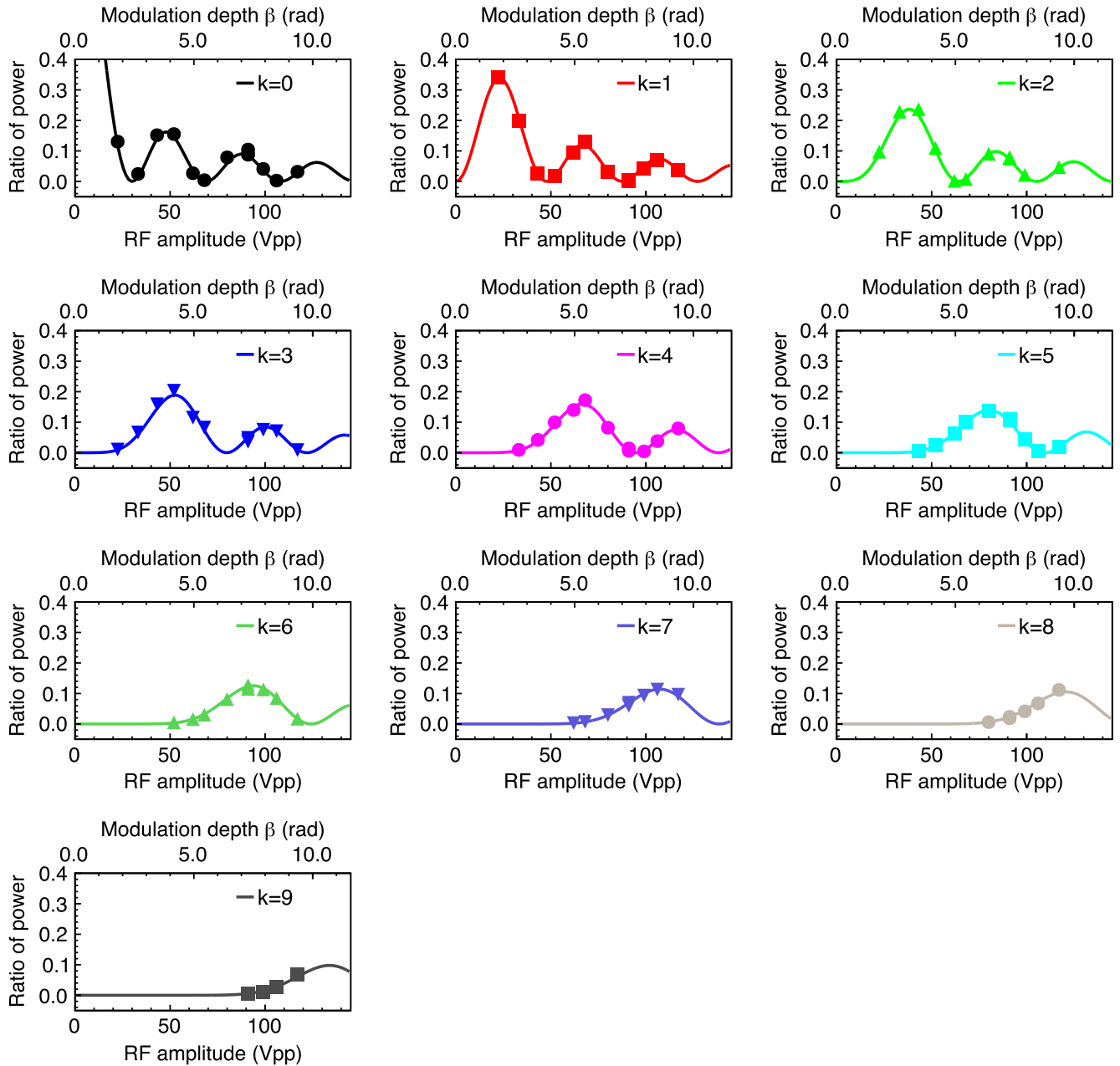
FIG. 5. Ratio of each sideband power to the incident power on the EOM as a function of the amplitude of the driving rf. Peak-to-peak amplitudes are shown on the horizontal axis. The legend indicates the order of the resolved sideband. Sidebands up to the ninth order can be identified and their optical powers can be described well by the theoretical model of phase modulation, which is represented as solid curves. The conversion factor F_{conv} from the rf amplitude to the modulation depth β was universal across all sideband orders and determined to be 0.080 rad/V_{pp} to ensure that the measurements agreed well with the theoretical predictions. β is indicated at the top of the horizontal axis. The maximum β confirmed in this test was 9.3 rad.

IV. MEASUREMENTS OF SPECTRAL AND TIMING CHARACTERISTICS

We operated the CPTG under the pulsed drive of the EOM, and measured the time-resolved spectrum of the pulse train by using a streak camera. Because the spectral shift was enhanced by an order of magnitude compared to the system in [19], direct observation of the time evolution of the laser spectrum became possible with the typical spectral resolution of the streak camera. Figure 6 shows the experimental setup of

the measurement. The laser was transmitted via a multimode optical fiber with a 200-μm core. The streak camera was operated in the single-sweep mode, which was triggered by a 10-Hz timing signal synchronized with the laser operation. Both the laser and trigger signals were transmitted over a distance of approximately 30 m. The laser light was dispersed in a 50-cm spectrometer with a grating with a groove density of 2400 mm^{-1} and blaze wavelength of 240 nm.

Figure 7 shows the typical time-resolved spectrum of the third harmonics of the CPTG, which is at 243 nm. In this
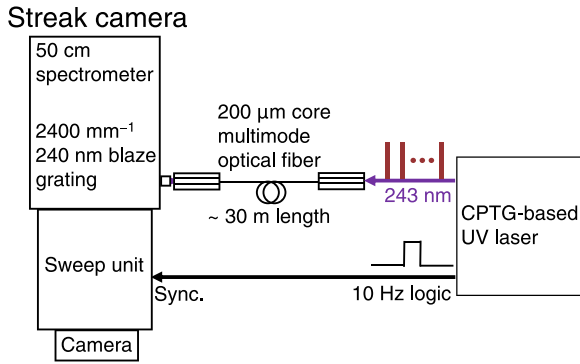
FIG. 6. Schematic setup for measuring the time-resolved spectrum using a streak camera.

measurement, the applied level of the rf peak-to-peak amplitude before the excitation of the CPTG was 14 V. In Fig. 7(a), we can observe two components with time durations of hundreds of nanoseconds, whose frequencies are individually higher and lower than the seed frequency. It is also clearly observed that both components shift away from the seed frequency. By fitting a linear chirp function to the time-resolved spectra, the chirp rates were estimated to be 6.2×10^2 and -5.2×10^2 GHz μs^{-1}. The results demonstrate that a chirp rate that is more rapid than required can be obtained using the upgraded pulsed phase modulation. Figure 7(b) shows the spectrum acquired by the short sweep time to achieve a time resolution sufficient for resolving each pulse in the train. Each chirped component formed a pulse train with a repetition rate the same as the EOM modulation frequency $f_m = 236$ MHz $= 1/4.23$ ns, not the longitudinal mode interval of the laser cavity. With a tripled modulation frequency when compared with the mode interval, six pulses from both components circulate simultaneously in the laser cavity. This is one of the different features when compared with the CPTG introduced in a previous study [19], wherein the modulation frequency coincided with the mode interval of the cavity, and two pulses circulated in the cavity. The time shift between two trains with opposite chirps was also directly observed as $\frac{1}{2f_m}$, as predicted by the theoretical model [19].

Because the up-chirp component is required for chirp cooling of Ps, we optimized the conversion efficiency of the THG for the up-chirp component by adjusting the phase-matching angles of the lithium triborate (LBO) (10-mm length) and beta barium borate (BBO) (4-mm length) crystals. Figure 8 shows a typical time-resolved spectrum of the optimized up-chirp component. The duration of the up-chirp component increased to approximately 300 ns because the phase-matching bands of both LBO and BBO crystals were centered in the frequency range of the up-chirp component sweeps. This duration is sufficiently long for chirp cooling of Ps from the typical initial temperature. Under this phase-matching condition, the down-chirp component weakened because its frequency was outside the phase-matching bandwidth. The linear chirp rate for the up-chirp component was estimated to be 6.3×10^2 GHz μs^{-1}. This result is consistent with the expected rate under the pulsed modulation of the EOM and is sufficiently rapid for realizing the optimized chirp cooling of Ps. The optimum chirp rate of 4.9×10^2 GHz μs^{-1} can also be achieved by adjusting

the amplitude of the driving rf signal after the excitation of the CPTG to a lower value or by finely adjusting the timing of its amplitude modulation.

Regarding the spectral width of each pulse, which is another important specification for the chirp cooling of Ps, we adopted another measurement method because the spectral resolution of the streak camera was not high enough to resolve the expected spectral width. We used a Fabry-Pérot etalon as an optical narrow bandpass filter at 243 nm, whose transmission frequency depends on the incident angle of light. The optical power spectrum was obtained from the transmittance through the etalon by scanning the incident angle. To resolve the spectrum of a single pulse, it is necessary to isolate the single optical pulse from the pulse train. The setup for the measurement is shown in Fig. 9. The incident and transmitted powers were measured using 350-MHz bandwidth Si biased detectors. Because the bandwidth was not wide enough to completely eliminate the falling tails of the preceding pulses, the pulse-chopping technique described in Fig. 3 using the acousto-optic modulator (AOM) and multipass amplifier was adopted to reduce the number of pulses detected. The typical time evolutions of the power measured at the input side are shown in Fig. 10. For the measurements reported hereinafter, the applied level of the rf peak-to-peak amplitude before the excitation of the CPTG was 30 V. The timing of the operation of the AOM and the excitation of the multipass amplifier can control the duration of the pulse train. To measure the spectral width of a single pulse, the shortest duration of the pulse train was adopted, as shown in Fig. 10(b). The chopping bandwidth was not wide enough to extract a single pulse in the train, which can have a duration of 300 ns for cooling Ps, as depicted in Fig. 10(a). However, the power of the first pulse in Fig. 10(b) decreased significantly such that the pileup effect on the pulse of interest was negligible.

Figure 11 shows the measured spectrum of a single pulse at around 150 ns in Fig. 10(a). We measured the instrumental function by measuring the transmission spectrum of the etalon using an SLM pulsed laser, which had a sufficiently narrow spectral width. The measurement was performed by varying the operating optical frequency. The SLM pulsed laser can be obtained from the CPTG without driving the EOM inside the laser cavity. The frequency after THG was estimated by tripling the measured frequency of the seed laser for the CPTG using a wavemeter with an accuracy of 60 MHz. By subtracting the spectral resolution, the spectral width of a single pulse constituting the cooling laser was estimated to be 8.9 GHz at FWHM, which is close to the designed value for the efficient chirp cooling and the applied $\beta = 2.4$ rad before the excitation of the CPTG. We also measured the spectral width of each pulse at other times from 0 to 300 ns using a 50-ns step, and the results were similar, ranging from 8.2 to 9.8 GHz at FWHM. This variation could originate from several factors such as the mismatch between the longitudinal mode interval of the CPTG cavity and the EOM modulation frequency, the mismatch between the seed laser frequency and the longitudinal mode, or the dispersion inside the cavity.

Another application of this technique for extracting a few pulses from the pulse train at an arbitrary timing is the measurement of the chirp rate using a high-resolution wavemeter. This measurement, which is complementary to that obtained by a streak camera, can be helpful, for example, in conducting
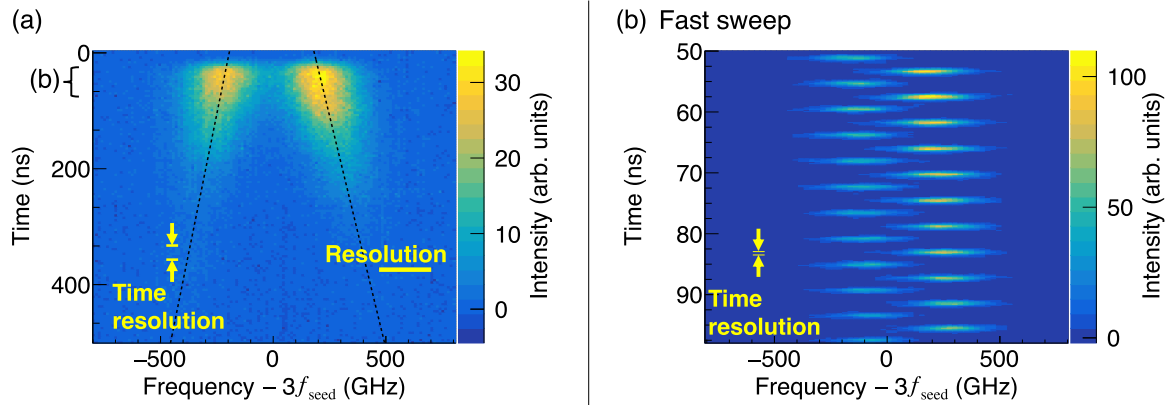
FIG. 7. Time-resolved spectra of the Ps cooling laser. (a) Spectrum acquired by setting the sweep time to observe all pulses in the train with a duration of hundreds of nanoseconds. Two components with frequencies higher and lower than those of the seed laser were observed. Either component chirps upward (up-chirps) or downward (down-chirps) so that the frequency shifts from the seed frequency become larger. The chirp rates were estimated to be 6×10^2 and -5×10^2 GHz μs^{-1} by fitting the linear functions to the spectral data. The fitted functions are superimposed on the spectrum (dashed lines). (b) Time-resolved spectrum at the beginning of the pulse train, acquired by fast sweeping to achieve better time resolution. The timing of the pulse trains of the two components are shifted by $\frac{1}{2}\frac{2\pi}{\Omega_m}$, as predicted by the theoretical model [19]. They were well synchronized with the timing of the pulsed drive of the EOM. Both (a) and (b) are averaged over 100 shots. The origin of the horizontal axis corresponded to the optical frequency of the third harmonic of the seed laser denoted as f_{seed}. The time resolutions were (a) 23 ns at FWHM and (b) 0.7 ns at FWHM. The frequency resolution was 2.3×10^2 GHz at FWHM in both spectra.

laser cooling experiments at a positron beam facility where a streak camera is not available. Figure 12 shows the frequency of the extracted pulse after taking the THG as a function of the extraction timing. The frequency was measured using a UV-compatible wavemeter with an accuracy of ± 15 GHz and a resolution of 40 GHz at 243 nm. We observed that the frequency of the pulse train starting from 292 GHz shifted from the tripled seed frequency, and the pulses were linearly chirped at an estimated rate of 4.7×10^2 GHz μs^{-1}. An optimal chirp rate of 4.9×10^2 GHz μs^{-1} was almost achieved; therefore, efficient chirp cooling was expected. The difference

from the result obtained using the streak camera originates from the difference in the modulation depth of the EOM and in the multipass amplifier in terms of the gain and amplification timing. The multipass amplifier was adjusted to ensure that the power of the pulse train was as uniform as possible over time.

With the achieved chirp rate and spectral width of each pulse, we expect that the laser cooling of Ps is possible considering realistic experimental parameters such as the initial temperature and velocity measurement capability. To estimate the area that can be irradiated with sufficient intensity by the laser to efficiently induce the $1S - 2P$ transition, we derived the effective power per spectral component of the laser and considered how the laser beam can be large at an intensity comparable to the saturation level. The required intensity per spectral component was assumed to be 0.45 W cm^{-2}, which is equivalent to the saturation intensity of the Ps $1S - 2P$
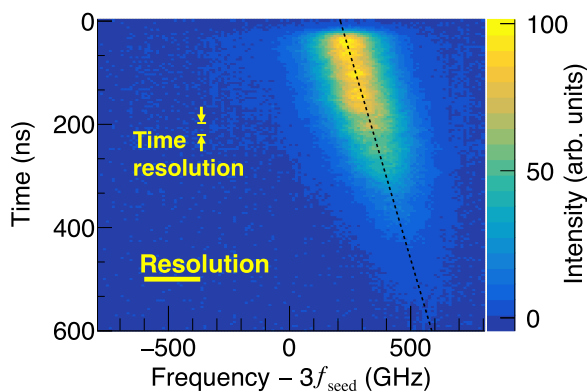

FIG. 8. Time-resolved spectrum with the up-chirp component optimized by adjusting the phase-matching angle. Because the phase-matching bands of both LBO and BBO crystals were centered in the frequency range of the up-chirp component, the THG efficiency for the chirping pulse train was maintained at a high value for a longer duration than that in Fig. 7(a). The estimated chirp rate was 6×10^2 GHz μs^{-1}, which was obtained by fitting the superposed linear model. The THG efficiency of the down-chirp component was so low that it could not be observed. The time resolution was 23 ns at FWHM, and the frequency resolution was 2.3×10^2 GHz at FWHM.
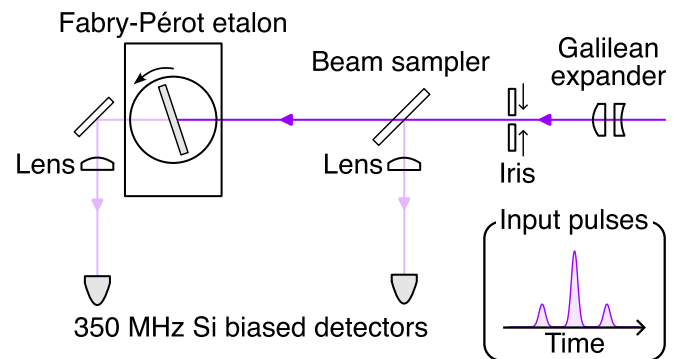

FIG. 9. Schematic setup for measuring the spectrum of a single pulse. The transmittance of each UV pulse was measured by scanning the etalon angle. To decrease the pileup effect due to the limited bandwidth of the detectors used in our setup, the output of the CPTG was chopped to reduce the number of pulses to be detected.
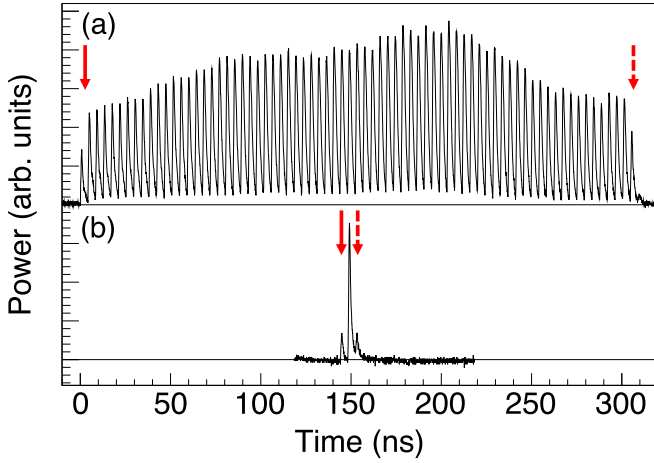
FIG. 10. Time-resolved optical power of the chopped pulse train at 243 nm. The turn-on timings of the AOM and excitation timing of the multipass amplifier are indicated by solid arrows, and the turn-off timings of the AOM are indicated by dashed arrows. The duration of the pulse train can be controlled to (a) 300 ns for the cooling of Ps and (b) approximately 12 ns to measure the spectral width of a single pulse. Three pulses are observed in (b). The optical power of the first pulse was decreased by pulse chopping to reduce the pileup effect on the second pulse, whose transmission spectrum was evaluated using an etalon.

FIG. 12. Optical frequency of each pulse constituting a UV pulse train. f_{SLM} denotes the frequency of the SLM operation, which is the same as the third harmonic of the seeded frequency of the CPTG. The filled diamonds show the center frequencies of the extracted pulses. A linear chirp was observed at a rate of $4.7 \times 10^2 \, \mathrm{GHz \, \mu s^{-1}}$, which was estimated by fitting a linear function (dashed line) to the data.
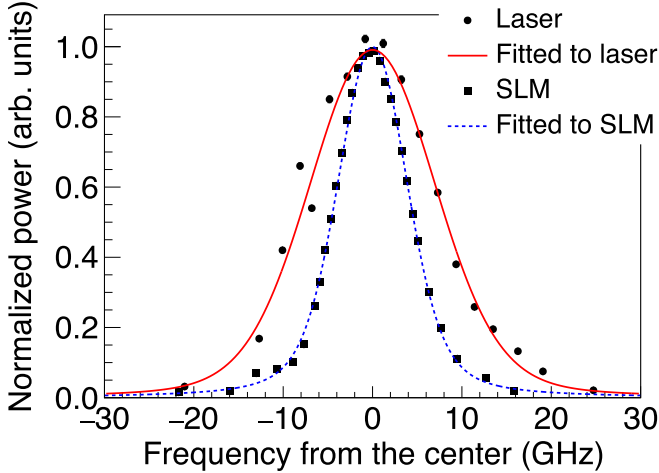

FIG. 11. Spectrum of a single pulse at approximately 150 ns in the pulse train and instrumental functions. The instrumental function was evaluated using the SLM operation of the CPTG with a narrow spectral width. The measured spectrum under the SLM operation is indicated by filled squares. The FWHM of the function was estimated to be 10 GHz by curve fitting with a Voigt function, as indicated by the dashed curve. The measured spectrum of a single pulse is indicated by the filled circles. The spectral width of a single pulse was estimated to be 8.9 GHz at the FWHM by subtracting the effect of the instrumental function. The subtraction was performed by the curve fitting of another Voigt function, assuming that the laser spectrum had a Gaussian line shape and was convolved with the instrumental function. The fitted function is indicated by the solid curve. The spectral peaks are intentionally shifted to the origin of the horizontal axis.
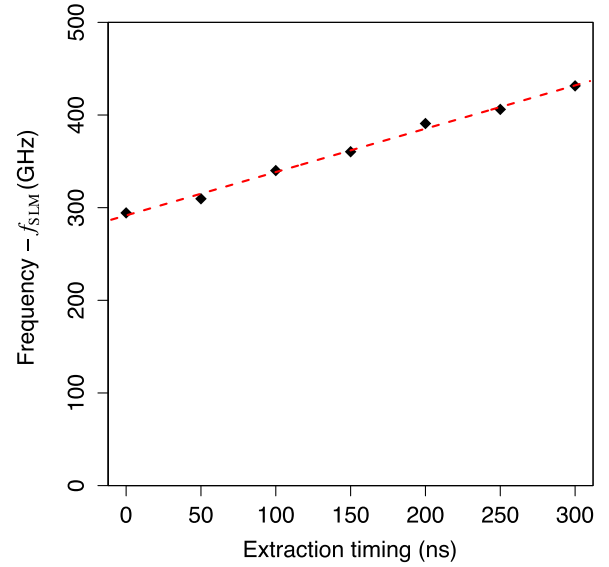
transition for light at the resonance frequency. This assumption was made considering that the frequency mode interval of the developed laser is comparable to the natural linewidth of the transition, as depicted in Fig. 4. With this interval, every Ps atom whose Doppler-shifted resonance frequency is within the envelope of the laser spectrum is effectively excited by nearly resonant light. Considering the duration of the pulse train τ and linear chirp rate R_c, the integrated spectral width is τR_c. The pulse energy per component of the laser spectrum with an interval of f_L is $\frac{U f_L}{\tau R_c}$, where U is the energy of the pulse train. Owing to the chirp, the effective duration of a single spectral component becomes shorter than the duration of the pulse train. With the spectral width of a single pulse δ, the effective duration can be estimated to be δ/R_c. Therefore, the effective peak power per spectral component is $\frac{U f_L}{\tau \delta}$. The parameters of the laser developed in this paper are $U = 700 \, \mathrm{J}$, $\tau = 300 \, \mathrm{ns}$, $f_L = 78.8 \, \mathrm{MHz}$, and $\delta = 8.9 \, \mathrm{GHz}$. The calculated effective power was 21 W and the corresponding area of laser irradiation at the saturation intensity was $46 \, \mathrm{cm^2}$. This area is sufficiently wide to cover a flight distance of approximately 2 cm for 300 ns with the most probable velocity at 300 K. Another aspect to consider is the extent to which the velocity distribution of Ps can be narrowed by chirp cooling. The frequency range that the laser sweeps due to the chirp is $4.7 \times 10^2 \, \mathrm{GHz \, \mu s^{-1}} \times 300 \, \mathrm{ns} = 1.4 \times 10^2 \, \mathrm{GHz}$. With two counterpropagating laser beams, Ps, whose Doppler shift for 243 nm is within the doubled frequency range as wide as $2.8 \times 10^2 \, \mathrm{GHz}$, can possibly be cooled to the recoil limit temperature. This range is more than half the FWHM ($4.6 \times 10^2 \, \mathrm{GHz}$) of the Doppler broadening profile at 300 K, and narrowing by chirp cooling can easily be detected by the well-established Doppler spectroscopy of Ps [24].

V. CONCLUSION

We developed a pulsed laser at 243 nm for the chirp cooling of Ps to near the recoil limit. Typically, the laser outputs a train of pulses whose carrier frequency was chirped at a rate of 4.7×10^2 GHz μs^{-1} and the spectral width was 8.9 GHz, both of which were directly confirmed by time-resolved spectroscopy measurements. Based on the fundamental properties of the chirp-cooling scheme for Ps, these parameters are appropriate for cooling as many Ps atoms as possible to the recoil limit temperature for laser cooling, which is 0.3 K for Ps. The key aspect of the laser development was enhancing the spectral broadening of the chirped pulse-train generator, which we developed for Ps cooling, by an order of magnitude. This enhancement was obtained by applying pulsed deep driving to the EOM. Further, the developed laser has a suitable pulse energy for laser cooling of Ps prepared at typical temperatures. The narrowing of the velocity distribution can be observed by the already established Doppler spectroscopy. The chirp cooling using the developed laser will pave the way for precision spectroscopy and achieving the BEC of Ps. The latter is among the ultimate applications of cold Ps. At the recoil limit temperature of approximately 0.3 K, the critical density of the BEC transition for the ideal noninteracting Ps gas is approximately 3×10^{15} cm^{-3} [7]. This density is close to that previously realized [25]. However, the chirp cooling to the recoil limit does not have a mechanism itself for the Ps gas to realize thermal equilibrium. This requires nontrivial studies about the formation process of the condensate. For example, if elastic interactions between Ps atoms are essential to realize thermal equilibrium of the Ps gas decelerated by the chirp cooling, the Ps gas should be created with a density higher than the critical value calculated for the ideal noninteracting gas. This is because the interaction rate should be large enough to realize thermal equilibrium within the short lifetime of Ps. Conversely, excessively high atomic densities can hinder the attainment of BEC conditions due to heating effects associated with photon reabsorption [26]. Although further studies are required to rigorously determine criteria for the BEC transition, the recoil limit temperature is so low that this chirp cooling could be a leap in Ps cooling, supporting attempts to achieve Ps BEC.

Note added. Recently, one-dimensional laser cooling of positronium was demonstrated [27,28]. The developed laser in this paper was utilized in [27].

[1] S. G. Karshenboim, Precision physics of simple atoms: QED tests, nuclear structure and fundamental constants, Phys. Rep. **422**, 1 (2005).

[2] G. S. Adkins, D. B. Cassidy, and J. Pérez-Ríos, Precision spectroscopy of positronium: Testing bound-state QED theory and the search for physics beyond the standard model, Phys. Rep. **975**, 1 (2022).

[3] D. B. Cassidy, Experimental progress in positronium laser physics, Eur. Phys. J. D **72**, 53 (2018).

[4] M. S. Fee, A. P. Mills, S. Chu, E. D. Shaw, K. Danzmann, R. J. Chichester, and D. M. Zuckerman, Measurement of the positronium $1^3S_1 - 2^3S_1$ interval by continuous-wave two-photon excitation, Phys. Rev. Lett. **70**, 1397 (1993).

[5] A. Ishida, T. Namba, S. Asai, T. Kobayashi, H. Saito, M. Yoshida, K. Tanaka, and A. Yamamoto, New precision measurement of hyperfine splitting of positronium, Phys. Lett. B **734**, 338 (2014).

[6] L. Gurung, T. J. Babij, S. D. Hogan, and D. B. Cassidy, Precision microwave spectroscopy of the positronium $n = 2$ fine structure, Phys. Rev. Lett. **125**, 073002 (2020).

[7] P. M. Platzman and A. P. Mills, Possibilities for Bose condensation of positronium, Phys. Rev. B **49**, 454 (1994).

[8] O. Morandi, P.-A. Hervieux, and G. Manfredi, Bose-Einstein condensation of positronium in silica pores, Phys. Rev. A **89**, 033609 (2014).

[9] K. Shu, X. Fan, T. Yamazaki, T. Namba, S. Asai, K. Yoshioka, and M. Kuwata-Gonokami, Study on cooling of positronium for Bose-Einstein condensation, J. Phys. B **49**, 104001 (2016).

[10] K. Shu, A. Ishida, T. Namba, S. Asai, N. Oshima, B. E. O'Rourke, and K. Ito, Observation of orthopositronium thermalization in silica aerogel at cryogenic temperatures, Phys. Rev. A **104**, L050801 (2021).

[11] F. Guatieri, S. Mariazzi, C. Hugenschmidt, and R. S. Brusa, Classical modeling of positronium cooling in silicon nanochannel plates, Phys. Rev. B **106**, 035418 (2022).

[12] S. Mariazzi, P. Bettotti, and R. S. Brusa, Positronium cooling and emission in vacuum from nanochannels at cryogenic temperature, Phys. Rev. Lett. **104**, 243401 (2010).

[13] F. Guatieri, S. Mariazzi, L. Penasa, G. Nebbia, C. Hugenschmidt, and R. S. Brusa, Time-of-flight apparatus for the measurement of slow positronium emitted by nanochannel converters at cryogenic temperatures, Nucl. Instrum. Methods Phys. Res. Sect. B **499**, 32 (2021).

[14] E. P. Liang and C. D. Dermer, Laser cooling of positronium, Opt. Commun. **65**, 419 (1988).

[15] T. Kumita, T. Hirose, M. Irako, K. Kadoya, B. Matsumoto, K. Wada, N. Mondal, H. Yabu, K. Kobayashi, and M. Kajita, Study on laser cooling of ortho-positronium, Nucl. Instrum. Methods Phys. Res. Sect. B **192**, 171 (2002).

[16] C. Zimmer, P. Yzombard, A. Camper, and D. Comparat, Positronium laser cooling in a magnetic field, Phys. Rev. A **104**, 023106 (2021).

[17] G. S. Adkins, R. N. Fell, and J. Sapirstein, Order α^2 corrections to the decay rate of orthopositronium, Phys. Rev. Lett. **84**, 5086 (2000).

[18] Y. Kataoka, S. Asai, and T. Kobayashi, First test of O(α^2) correction of the orthopositronium decay rate, Phys. Lett. B **671**, 219 (2009).

[19] K. Yamada, Y. Tajima, T. Murayoshi, X. Fan, A. Ishida, T. Namba, S. Asai, M. Kuwata-Gonokami, E. Chae, K. Shu, and K. Yoshioka, Theoretical analysis and experimental demonstration of a chirped pulse-train generator and its potential for efficient cooling of positronium, Phys. Rev. Appl. **16**, 014009 (2021).

[20] A. M. Alonso, B. S. Cooper, A. Deller, S. D. Hogan, and D. B. Cassidy, Positronium decay from $n = 2$ states in electric and magnetic fields, Phys. Rev. A **93**, 012506 (2016).

[21] V. Balykin, V. Letokhov, and V. Mushin, Observation of the cooling of free sodium atoms in a resonance laser field with a scanning frequency, Pis'ma Zh. Eksp. Teor. Fiz. **29**, 614 (1979) [JETP Lett. **29**, 560 (1979)].

[22] J. V. Prodan and W. D. Phillips, Chirping the light-fantastic? Recent NBS atom cooling experiments, Prog. Quantum Electron. **8**, 231 (1984).

[23] C. Cohen-Tannoudji, *Frontiers in Laser Spectroscopy* (North-Holland, Amsterdam, 1977), Vol. 1, pp. 3–104.

[24] D. B. Cassidy, P. Crivelli, T. H. Hisakado, L. Liszkay, V. E. Meligne, P. Perez, H. W. K. Tom, and A. P. Mills, Positronium cooling in porous silica measured via Doppler spectroscopy, Phys. Rev. A **81**, 012715 (2010).

[25] D. B. Cassidy and A. P. Mills, Physics with dense positronium, Phys. Status Solidi C **4**, 3419 (2007).

[26] A. Urvoy, Z. Vendeiro, J. Ramette, A. Adiyatullin, and V. Vuletić, Direct laser cooling to Bose-Einstein condensation in a dipole trap, Phys. Rev. Lett. **122**, 203202 (2019).

[27] K. Shu, Y. Tajima, R. Uozumi, N. Miyamoto, S. Shiraishi, T. Kobayashi, A. Ishida, K. Yamada, R. W. Gladen, T. Namba, S. Asai, K. Wada, I. Mochizuki, T. Hyodo, K. Ito, K. Michishio, B. E. O'Rourke, N. Oshima, and K. Yoshioka, Laser cooling of positronium, arXiv:2310.08761.

[28] L. T. Glöggler, N. Gusakova, B. Rienäcker, A. Camper, R. Caravita, S. Huck, M. Volponi, T. Wolz, L. Penasa, V. Krumins, F. P. Gustafsson, D. Comparat, M. Auzins, B. Bergmann, P. Burian, R. S. Brusa, F. Castelli, G. Cerchiari, R. Ciuryło, G. Consolati *et al.* (AEḡIS Collaboration), Positronium laser cooling via the $1\,^3S$-$2\,^3P$ transition with a broadband laser pulse, Phys. Rev. Lett. **132**, 083402 (2024).